# A proper simulation of the landfast ice in the Kara Sea slows down the Atlantification of the Eurasian Basin

Yuqing Liu[1*], Martin Losch[1*], Bruno Tremblay[2] and Markus Janout[1]

[1*]Alfred-Wegener-Institut, Helmholtz-Zentrum für Polar-und Meeresforschung, 27570, Bremerhaven, Germany.
[2]Department of Atmospheric and Oceanic Sciences, McGill University, H3A 0B9,Montreal, Quebec, Canada .

*Corresponding author(s). E-mail(s): Yuqing.Liu@awi.de; Martin.Losch@awi.de;
Contributing authors: Bruno.Tremblay@mcgill.ca; Markus.Janout@awi.de;

**Abstract**

Observations show an Atlantification of the Eurasian Basin of the Arctic Ocean, with deeper penetration, shoaling and ventilation of Atlantic waters in the eastern Arctic and an associated weakening of the cold halocline layer. All of these factors have a profound impact on the sea ice cover above and potentially on the transition of the Arctic to a seasonal ice cover. Here we show, using a coupled ice-ocean model, that a proper simulation of the landfast ice cover in the relatively small but deeper peripheral Kara Sea has a disproportionately large influence on the halocline stability in the Eurasian basin and beyond. Specifically, the presence of landfast ice in the Kara Sea reduces ice growth and therefore salt rejection into the surface ocean. This negative salinity anomaly is advected eastward along the continental shelf in the Makarov Basin and then out of the Arctic through Fram Strait by the Transpolar Drift Stream on timescales of less than ten years. Global Climate Models, however, do not yet include landfast ice parameterizations and therefore are missing this key process affecting the halocline stability,

Atlantification of the Makarov Basin, and potentially the timing of a seasonally ice-free Arctic.

**Keywords:** Landfast ice, Arctic hydrography, Lateral drag parameterization

# 1 Introduction

Landfast ice (LFI) – sea ice that stays fast along the coast where it is attached to the shore or over shoals [1] – can extend a few kilometers (e.g., Beaufort Sea, Western Laptev Sea) to several hundred kilometers into the ocean (e.g., Kara Sea, East Siberian Sea, Eastern Laptev Sea). Its presence is associated with specific bathymetry and coastline features; for instance, it can be grounded on the ocean floor by pressure ridges in shallow water and over shoals (Stamukhi) [2–7], attached to coastlines by local tensile force or compressive forces from distant land protrusion along the coast [8], or supported by offshore islands [9]. LFI plays an important role in polar coastal regions by decreasing the energy, momentum, and heat flux between the atmosphere and the ocean, and therefore reducing surface ocean mixing [4, 10–12]. This extension of the land also provides a platform for hunting, tourism, scientific research, oil and gas exploration, and serves as a habitat for polar wildlife [13–16].

At the seaward end of LFI, flaw-lead polynyas [5] form as openings between stationary fast ice and mobile pack ice, where large air-sea heat fluxes, sea ice growth, and associated salt rejection lead to the formation of dense waters. The cold dense waters in turn spill over the continental shelves, and find their level of equilibrium between the warm salty Atlantic and the cold fresher surface water, forming the cold halocline layer [17, 18]. This cold halocline layer acts as a buffer between the two water masses, leading to significant sea ice growth in winter and the formation of a perennial sea ice cover — that is, surface convection of cold and saltier surface waters driven by ice growth and brine rejection sink to the based of the mixed layer and bring (still) cold halocline water at the freezing point into the mixed layer, and therefore does not lead to vertical transport of ocean heat, in contrast with the Southern Ocean where the thermocline coincides with the halocline [19]. The recent Atlantification of the Eurasian Basin, that is, the eastward progression of warmer Atlantic Water into the eastern Arctic, has led to shoaling of the intermediate-depth Atlantic Water layer and a weakening of the halocline, increasing ocean-interior ventilation in winter [20, 21]. Subsequently, the associated enhanced release of oceanic heat reduced winter sea ice formation in the Eurasian Basin [22]. A previous retreat of the cold halocline layer in the early 1990's [23] followed a peak positive phase of the Arctic Oscillation so that the Eurasian river runoff formed a fresh coastal current and did not spread over the entire shelf. Thereby, the shelf hydrography and the formation of the cold halocline waters in the Makarov Basin were affected [24]. Should the cold halocline disappear, the Atlantification of the Arctic would ventilate significant Atlantic water heat in winter leading to a seasonal sea ice cover in the Eurasian Basin [25].

In this work, evidence is presented for a significant impact of an LFI cover in the Kara Sea — a feature that is missing in current Earth System Models because of the absence of fast ice parameterizations — on the local salt budget. This salinity anomaly signal in turn is advected out of the Kara Sea and weakens the stability of the halocline over the entire Eurasian Basin.

# 2 Results

## 2.1 More landfast ice in the Kara Sea, fresher surface water in the interior Arctic

We activate different parameterizations of LFI that result in the presence or absence of LFI in specific parts of the model domain (see Methods section 5). More LFI makes the shelves fresher [17], but more LFI in the Kara Sea also makes the interior Arctic fresher (Figure 1). This negative salinity anomaly in the interior Arctic Ocean reduces a salinity bias relative to observations. To illustrate this, we compute the root-mean-square difference between an average of 20 salinity casts from the Unified Database for Arctic and Subarctic Hydrography (UDASH) [26, 27] and the model solutions. The casts were collected in all Aprils of our simulation period of 2006–2015 in the region between 120°–180°E and north of 75°N (approximately the Makarov Basin). The root-mean-square difference for the simulations with LFI is 1.06 and the corresponding value for the control run (CTRL) is 1.27, so that the extra fast ice in the Kara Sea and the consequential negative salinity anomaly in the Makarov Basin slightly reduces a model bias.

The simulation with the fast ice parameterization (Figure 1b) produces higher ice concentration (less open water for sea ice formation) along the coastlines in the Beaufort, East Siberian, Laptev and Kara Seas, and lower ice concentration (more open water for more sea ice formation in flaw lead polynyas) offshore in accord with results from [17]. The presence of LFI leads to fresher surface water in the simulations with fast ice parameterization compared to the control simulation (Figure 1b), because the stable LFI cover inhibits new ice formation. This is particularly evident in the Laptev and East Siberian seas (Figure 1b). As a consequence, less salt is rejected, reducing the salinity of the surface ocean. Northward of the LFI edge in the East Siberian Sea, the upper ocean is more saline than in the control simulation, again in accord with previous results from [17]. During offshore wind events in the East Siberian Sea, new ice formation at the edge of the LFI leaves more salt behind and increases the local surface ocean salinity. In the Kara Sea, the additional LFI parameterization [8] leads to an LFI cover also present in the Kara Sea where the water is deeper and ice keels alone fail to stabilize the LFI cover (Figure 1b). In contrast to the shallow East Siberian and Laptev Seas, LFI in the deep marginal Kara Sea leads to a much fresher upper ocean that spills over to the Makarov Basin through Vilkitsky Strait (between

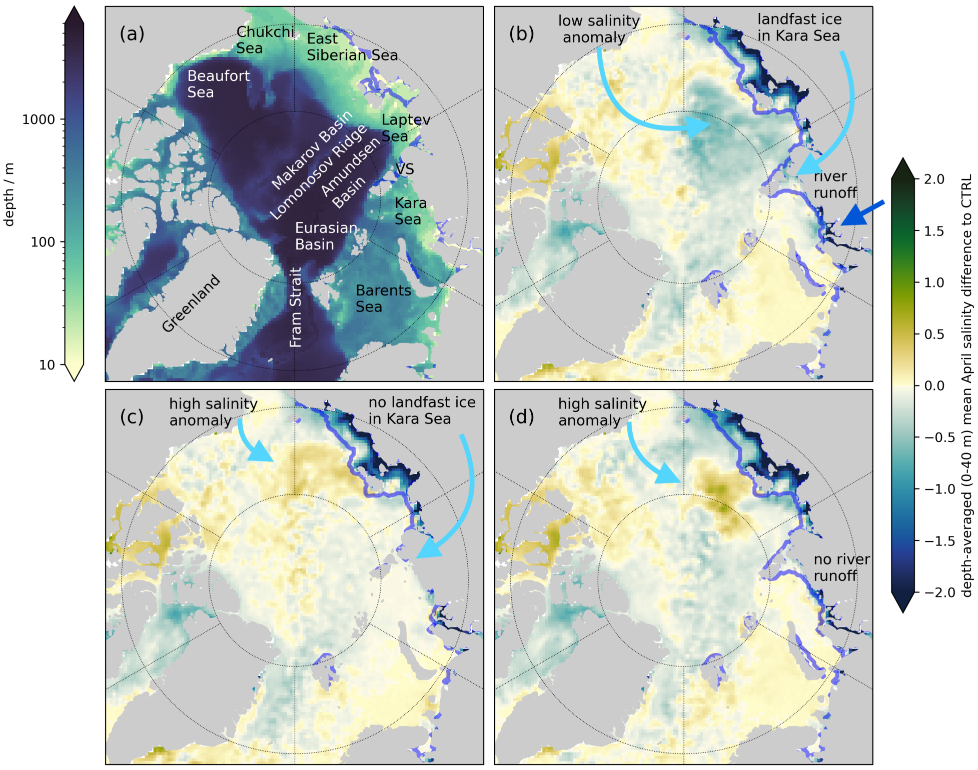


**Fig. 1** (a) Arctic topography. VS denotes the Vilkitsky Strait. The blue contour line denotes the (poorly) simulated fast ice extent in the control run (CTRL, without fast ice parameterization). (b)–(d) Depth averaged (0–40 m) salinity differences for the mean April of 2006–2015: (b) between the simulation with all fast ice parameterizations, i.e., with a realistic LFI distribution as indicated by the blue contour line, and CTRL simulation; (c) the same as (b), but with the lateral drag parameterization turned off explicitly in the Kara Sea; there is no LFI in the Kara Sea as indicated by the blue contour line; (d) the same as (b), but without river runoff in the Kara Sea and in CTRL; there is slightly less LFI in the Kara Sea as indicated by the blue contour line.

the Laptev and Kara Seas, Figure 1b). We emphasize that this is almost entirely caused by LFI in the Kara Sea. In a simulation where the new LFI parameterization is turned off, no LFI in the Kara Sea is present and the fresh anomaly in the Makarov Basin disappears (Figure 1c).

The amplitude of the negative salinity anomaly in the Kara Sea and the Makarov Basin decreases in an experiment where the river runoff in the Kara Sea is turned off (in both control and sensitivity experiments) and a positive anomaly appears north of the New Siberian Islands (Figure 1d). This suggests that the river runoff also contributes

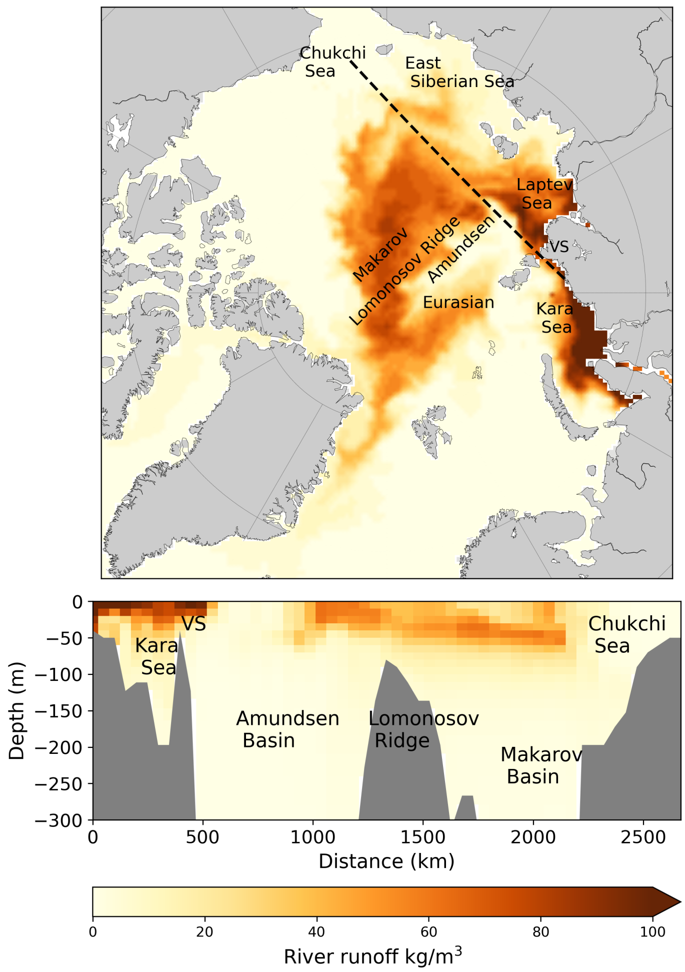


**Fig. 2** (a) Depth averaged (0–40 m) passive tracer of the river runoff from the Kara Sea in April 2015 in the control run. (b) Vertical distribution of the passive tracer along a section marked by the dashed line in panel (a) starting from the Kara Sea into the Chukchi Sea.

to transporting the low salinity signal in the upper ocean from the Kara Sea to the Makarov Basin (Figure 2).

To corroborate this speculation, we trace the river runoff from the Ob and Yenisei Rivers in the Kara Sea with a passive tracer (Figure 2). The passive tracer exits the Kara Sea through the Vilkitsky Strait, with a portion entering the Laptev Sea while the remainder subducts into the Amundsen and Makarov Basins. The tracers are then advected by the Transpolar Drift Stream over the Lomonosov Ridge and finally

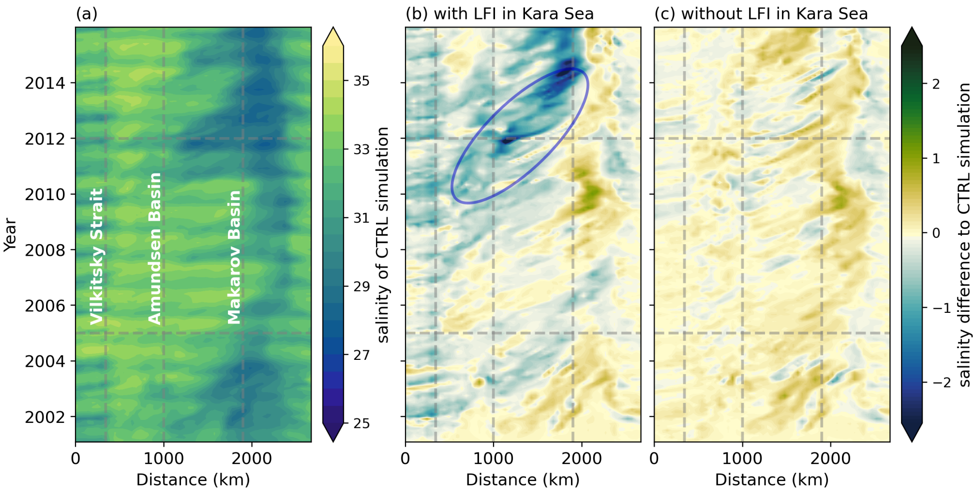


**Fig. 3** Hovmöller diagram along the dashed line in Figure 2a for years 2001 to 2015 (2001–2005 is a spin-up) of depth-averaged (0–40m) (a) salinity in the control simulation (CTRL); (b) salinity difference between the simulation with LFI in the Kara Sea) and the control simulation (corresponding to Figure 1b); (c) salinity difference between the simulation without LFI in the Kara Sea and the control simulation (corresponding to Figure 1c). The blue ellipse marks the strong negative salinity anomaly described in the text. The x-axis is the distance in kilometers along the transect (dashed line) in Figure 2a. The dashed vertical lines parallel to the y-axis indicate the approximate locations of the Vilkitsky Strait, the Amundsen and the Makarov Basins (from left to right), and the lower dashed horizontal lines mark the end of the spin-up and the the upper ones the beginning of the large positive salinity anomaly in 2012.

exit through Fram Strait (Figure 2). The passive tracer of the Ob and Yenisei water has a similar distribution to the observed Ob and Yenisei water based on chemical tracer-based water mass analyses [28, their Figure 3b]. The tracer pattern is also very similar to the pattern of the low salinity signal in the upper ocean (Fig. 1), implying a freshwater transport path from the Kara Sea to the Makarov Basin.

A Hovmöller diagram along the dashed line in Figure 2a of the depth-averaged (0–40 m) salinity and salinity difference between different experiments illustrates the transport of the low salinity signal from the Kara Sea to the Chukchi Sea (Figure 3). The difference between simulations with and without LFI in the Kara clearly shows that salinity anomalies in the Makarov Basin originate from the Kara Sea, and that local salinity anomalies in the Laptev or East Siberian seas are not responsible for the negative salinity anomaly in the Makarov Basin.

Very early in the simulation without without LFI in the Kara Sea, a positive salinity anomaly at the edge of the polynya in the Laptev and East Siberian seas develops locally (1500–2200 km, after 2001 during the spinup, Figure 3c), because new ice formation releases salt into the ocean. This anomaly persists until the end of the simulation (see also light blue arrow in Figure 1c). The same positive salinity anomaly in the Makarov Basin also appears early in the simulation with LFI in the Kara Sea (Figure 3b). But here, and in contrast to the locally generated signal, low salinity of the Kara Sea is advected to the Makarov and Eurasian Basins as early as 2002. There are smaller pulses of negative salinity anomaly moving from the Kara Sea to the Makarov Basin throughout 2001–2007. This process increases in 2008, with a negative salinity anomaly peak in 2012 (blue ellipse in Figure 3b).

## 2.2 Salt budget analysis

The salt content in the Arctic Ocean is determined by surface forcing, advection, and to a very small extent by diffusion between the surface and deeper ocean layer (see Methods section 5). The differences in salt content, salt advection and diffusion between the simulation with and without LFI parameterization in the Kara Sea are small when integrated over the entire model domain ($O(< 1\%)$ of the signal, results not shown). In the upper 40 m of the Makarov Basin, the mean salt content changes very little over time in the CTRL simulation, but in the cumulative budget the considerable horizontal advection of salt is balanced by downward vertical advection out of the 40 m surface layer. Vertical diffusion and surface fluxes are small (Figure 4a).

In the simulation without LFI only in the Kara Sea, the additional LFI in other marginal seas (Figure 1c), less sea ice formation and salt release into the ocean is advected into the Makarov Basin, especially after 2012. This decrease of horizontal advection is balanced by reduced downward vertical advection of salt, leaving the mean salt practically unchanged (Figure 4b, thick lines). The reduction of salt advected in

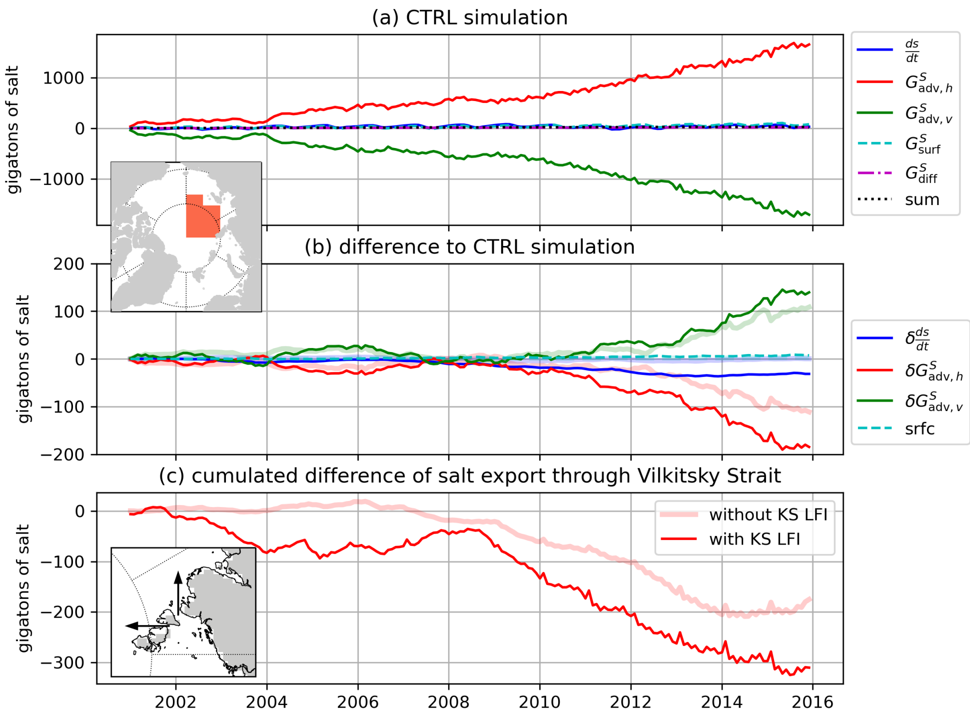


**Fig. 4** Time series of (a) accumulated salt budget terms ($\int_0^t G(t')\,dt'$, see Eq. 1 in the Methods section) for the top four layers (40 m) of the Eurasian and Makarov Basin (see red area in the inset) for the CTRL simulation. The horizontal advection of salt ($G^S_{\mathrm{adv,h}}$) is balanced by vertical advection ($G^S_{\mathrm{adv,v}}$) (b) difference of simulations without and with LFI in the Kara Sea. With LFI (but not in the Kara Sea) the horizontal advection of salt is reduced, balanced by a reduction of downward advection (faint thick lines). With LFI also in the Kara Sea the downward advection decreases less than the horizontal advection, potentially because of increased stability, so that these terms no longer balance and the net salt content reduces (thin lines). (c) difference of accumulated salt flux relative to CTRL through the Vilkitsky Strait (in gigatons of salt, negative values mean a reduced salt flux). The flux is the combination of the flux through the actual Vilkitsky Strait and a small northward opening (see inset); red thin line: with LFI in the Kara Sea (KS); thick line: without LFI in the Kara Sea.

the Makarov Basin is even larger with LFI present in the Kara Sea (after 2008 and 2012), but in this case is not balanced entirely by a reduction in downward vertical advection, probably because of an increase in surface stratification and the mean salinity (Figure 4b, thin lines). The local reduction in horizontal advection between 2004 and 2008 is offset by vertical advection in this simulation supporting the notion that the magnitude of the horizontal advection anomaly is important in this balance and can lead to non-linear effects. The salt flux leaves the Kara Sea mainly through the Vilkitsky Strait (Figure 4c). In the simulation with LFI in the Kara Sea, an approximate 100 gigatons of salt are not advected out of the Kara Sea through the Vilkitsky Strait (Figure 4c), in line with the deficit of advected salt in the Makarov Basin.

# 3 Discussion

The presence or absence of landfast ice (LFI) in sea ice-ocean models significantly changes the position of offshore polynyas and hence the location where sea ice forms over open water. The altered freshwater flux affects the salinity forcing which in turn impacts the stability of the halocline [17]. These findings were derived from a numerical model that lacked LFI representation in the Kara Sea. Here, we improved the representation of LFI in the Kara Sea – a relatively small Arctic marginal seas – by incorporating an additional lateral drag parameterization [8] addressing issues where previous methods had failed [3, 17]. This parameterization can be activated or deactivated using a single parameter (coastline roughness), allowing for the inclusion or exclusion of LFI in the Kara Sea. Moreover, it can be selectively deactivated in specific regions as needed. The results presented above are robust with respect to the specific modifications in physics used to simulate landfast ice in the Kara Sea, whether through a lateral drag or increased shear and tensile strength [18, 29] of the sea ice.

The presence or absence of LFI in the Kara Sea on the Makarov Basin hydrography is surprisingly large given its size compared with other (closer) marginal seas (e.g., Laptev, East Siberian, Beaufort Sea). For the halocline, the significant decrease in salinity within the top 40 meters of the water column enhances the stability of the water column, while also correcting a known saline model bias. Similarly, a reduction in LFI in the Kara Sea —— driven, for example, by climate change —— could decrease stability in the central Arctic Ocean, potentially accelerating Atlantification. This would allow warmer Atlantic waters to more easily reach the surface [30, 31], with profound implications for sea ice extent and seasonality.

Although the negative surface salinity anomaly in the simulation with LFI in the Kara Sea travels from the Kara Sea to the Makarov Basin soon after the start of the model run, there are two main transport anomaly episodes (2002–2006 and 2008–2015) driven by punctual wind-forcing anomalies [32, 33]. The negative salinity difference in the upper ocean is largest after the end of summer in 2012 (Figure 3b), presumably because of the large sea ice retreat in 2012. In August 2012, an intense storm increased mixing in the ocean boundary layer, increased upward ocean heat transport, causing bottom melt, and reduced the sea ice volume about twice as fast as in other years [34]. Eventually, the sea ice extent at the end of the summer in 2012 was smaller than it had been since the beginning of the satellite record in the late seventies [35]. These processes were also at play in our simulation and the mean simulated sea ice extent reached its lowest value of the simulation in 2012 (not shown).

The Kara Sea receives freshwater discharge from the Ob and Yenisei Rivers, which carry over one-third of the total freshwater discharge in the Arctic [36]. The geostrophic surface currents determine the circulation pathways of river runoff and of surface water originally from the Pacific and the Atlantic Oceans [37]. The simulated passive tracer for Ob and Yenisei water agrees with the observed Ob and Yenisei water distribution [28, 38]. The tracer experiment demonstrates how the river runoff and the negative salinity anomaly in the upper ocean, initially induced by the LFI in the Kara Sea, travel from the Kara Sea to the Makarov Basin via the Vilkitsky Strait (Figure 2). In our simulations, the LFI in the Kara Sea leads to a deficit of about 100 gigatons of salt leaving the Kara Sea by the end of the simulation (Figure 4c). The exact mechanism by which the river runoff in the Kara Sea modifies the influence of the LFI on the hydrography cannot be extracted from the numerical model because the Ob and Yenisei water is stored in LFI during sea ice formation. Further, the riverine heat, which is not considered in our model, is believed to be important to explain the phenomena [39].

The Arctic mixed layer is important to physical, chemical, and biological processes. Mixed layer properties also influence ocean stratification, sea ice distribution, and heat transfer between ocean, sea ice, and atmosphere. Two possible drivers for the change of the seasonal mixed layer depth are sea ice thermodynamics (i.e., salt rejection during ice formation, freshwater input during ice melt) and wind-driven mixing [40]. During ice-free phases, wind-driven mixing deepens the mixed layer, while thermodynamic processes dominate the stratification and control mixed layer depth variability in winter. With more LFI, less new ice is formed and less salt is released into the ocean which may modify the mixed layer depth. Studying the details of the interaction of LFI with mixed layer dynamics would require a dramatically refined vertical grid and even Large Eddy Simulations.

# 4 Conclusion

LFI in the Kara Sea changes the surface salinity of the central Arctic on timescales of a few years. In general, more LFI in the Arctic Ocean decreases the upper ocean salinity locally on the shelves in the Kara, Laptev, and East Siberian Seas. The largest effect, however, is found for the Kara Sea. Here, the relatively small LFI area induces a fresh anomaly in the upper ocean that is transported to the central Arctic Ocean where it leads to a surprisingly large salinity anomaly that increases the halocline stability. River runoff in the Kara Sea contributes to transporting the signal from the Kara Sea to the Makarov Basin. The negative salinity tendency with the LFI in both shallow and deep shelves can be attributed mainly to reduced advective fluxes of salt that are not balanced by reduced vertical advective fluxes. These mechanisms become apparent after implementing a combination of a lateral and a basal drag parameterization in a pan-Arctic sea ice model to improve the simulation of LFI in the Arctic.

A sea ice model with a proper representation of LFI will improve our understanding of its influence on the hydrography in the Arctic. Our model simulations suggest that LFI in the Kara Sea stabilizes the water column in the central Arctic. Once the LFI in the Kara Sea disappears due to a warming Arctic, the stabilizing effect reduces within a few years and the Atlantificiation of the Arctic can accelerate.

# 5 Methods

We use a regional Arctic configuration of the Massachusetts Institute of Technology general circulation model (MITgcm) [41, 42] with a grid resolution of 36 km. This model resolves ocean and sea ice processes with a finite-volume discretization on an Arakawa C grid. The sea ice component includes zero-layer thermodynamics [43] and viscous-plastic dynamics with an elliptical yield curve and a normal flow rule [44, 45]. The model is forced by atmospheric fields from the global atmospheric reanalysis ERA-Interim data set [46]. The hydrography is initialized with temperature and salinity fields from the Polar Science Center Hydrographic Climatology 3.0 [47]. Details of the sea ice model can be found in [48, 49].

Without an explicit parameterization of LFI, sea ice models grossly underestimate the LFI extent. We implement two fast ice parameterizations: a basal drag (BD) parameterization [3] leads to realistic LFI areas in shallow marginal seas such as the Beaufort, Laptev and the East Siberian Seas, and a new fast ice parameterization where an explicit lateral drag (LD) that depends on the sub-grid-scale coastline length and orientation replaces the no-slip boundary condition of the sea ice momentum equations [8]. The latter parameterization leads to more LFI in the relatively deep Kara Sea, where the basal drag parameterization that relies on relatively shallow depths fails. Thus, the new parameterization can be used as a switch to turn on or off the LFI cover in the Kara Sea and other selected regions of the Arctic Ocean [8]. A control simulation (CTRL) without fast ice parameterization grossly underestimates

LFI extent and timing. We make use of the fast ice parameterizations so that we can compare simulations with realistic LFI in all relevant regions and simulations where the parameterizations are turned off in selected regions such as the Kara Sea to the control simulation. For each configuration, the model is run from 2001 to 2015. The first five years constitute a spin-up during which the sea ice and surface ocean reach stable states for analysis.

Integrating the salt conservation equation leads to a salt budget equation. The change in salt content over time ($G^S_{\mathrm{tot}}$) in a given volume $V$ with total surface area $A$ and interface area with the atmosphere $A_{\mathrm{surf}}$ is equal to the convergence of the advective ($G^S_{\mathrm{adv}}$) and diffusive fluxes $F_{\mathrm{diff}}$ ($G^S_{\mathrm{diff}}$), and a forcing term associated with surface salt flux $F_{\mathrm{forc}}$ ($G^S_{\mathrm{forc}}$):

$$\underbrace{\frac{\partial s}{\partial t}}_{G^S_{\mathrm{tot}}} = \underbrace{-\rho \oint_A uS\,da}_{G^S_{\mathrm{adv}}} + \underbrace{\rho \iiint_V F_{\mathrm{diff}}\,dx\,dy\,dz}_{G^S_{\mathrm{diff}}} + \underbrace{\rho \iint_{A_{\mathrm{surf}}} F_{\mathrm{forc}}\,dx\,dy}_{G^S_{\mathrm{forc}}}, \quad (1)$$

where $\mathbf{u}$ is the ocean velocity normal to the area, $S$ is the salinity (in grams per kilograms of sea water), $s = \rho \iiint_V S\,dx\,dy\,dz$ is the salt content (in grams), $\rho = 1035\,\mathrm{kg\,m^{-3}}$ is the sea water reference density, $da$ is the area element. For our analysis we split the advective contribution into a horizontal $G^S_{\mathrm{adv,h}}$ and a vertical part $G^S_{\mathrm{adv,v}}$. Integrating Eq. 1 gives the accumulated salt contents $\int_0^t G(t')\,dt'$ for each term.


## Acknowledgments

The authors thank Thomas Jung, and Lars Kaleschke for constructive discussions.


# Declarations


*Funding:* This work is supported by the DFG-funded International Research Training Group ArcTrain (IRTG 1904 ArcTrain).

*Data availability:* The salinity in the Unified Database for Arctic and Subarctic Hydrography (UDASH) is available from the PANGAEA data archive [26].

*Code availability:* The model data in this manuscript is based on the Massachusetts Institute of Technology general circulation model (MITgcm) [42], the version with lateral drag parameterization is available at https://doi.org/10.5281/zenodo.7954400 and the model configurations at https://doi.org/10.5281/zenodo.7919422.

*Authors' contributions:* YL and ML designed the experiments, YL carried them out and analyzed the data under the supervision of ML and BT. YL wrote the manuscript with contributions from ML, BT, and MJ.

## References


[1] World Meteorological Organization. WMO sea-ice nomenclature. Terminology, codes and illustrated glossary. Tech. Rep., Secretariat of the World Meteorological Organization, Geneva (1970).

[2] Mahoney, A. R., Eicken, H., Gaylord, A. G. & Gens, R. Landfast sea ice extent in the Chukchi and Beaufort Seas: The annual cycle and decadal variability. *Cold Regions Science and Technology* **103**, 41–56 (2014).

[3] Lemieux, J. F. *et al.* A basal stress parameterization for modeling landfast ice. *Journal of Geophysical Research: Oceans* **120**, 3157–3173 (2015).

[4] Lemieux, J. F. *et al.* Improving the simulation of landfast ice by combining tensile strength and a parameterization for grounded ridges. *Journal of Geophysical Research: Oceans* **121**, 7354–7368 (2016).

[5] Rabault, J. *et al.* A dataset of direct observations of sea ice drift and waves in ice. *Scientific Data* **10**, 251 (2023).

[6] Kasper, J. L. & Weingartner, T. J. The spreading of a buoyant plume beneath a landfast ice cover. *Journal of Physical Oceanography* **45**, 478–494 (2015).

[7] Plante, M., Tremblay, B., Losch, M. & Lemieux, J.-F. Landfast sea ice material properties derived from ice bridge simulations using the maxwell elasto-brittle rheology. *The Cryosphere* **14**, 2137–2157 (2020).

[8] Liu, Y., Losch, M., Hutter, N. & Mu, L. A new parameterization of coastal drag to simulate landfast ice in deep marginal seas in the arctic. *Journal of Geophysical Research: Oceans* **127**, e2022JC018413 (2022).

[9] Divine, D. V., Korsnes, R., Makshtas, A. P., Godtliebsen, F. & Svendsen, H. Atmospheric-driven state transfer of shore-fast ice in the northeastern Kara Sea. *Journal of Geophysical Research C: Oceans* **110**, 1–13 (2005).

[10] Johnson, M. *et al.* Evaluation of Arctic sea ice thickness simulated by Arctic Ocean model intercomparison project models. *Journal of Geophysical Research: Oceans* **117** (2012).

[11] Fraser, A. *et al.* Antarctic landfast sea ice: A review of its physics, biogeochemistry and ecology. *Reviews of Geophysics* **61**, e2022RG000770 (2023).

[12] Cornish, S. *et al.* Rise and fall of sea ice production in the arctic ocean's ice factories. *Nature Communications* **13**, 7800 (2022).

[13] Labrousse, S. *et al.* Where to live? landfast sea ice shapes emperor penguin habitat around antarctica. *Science Advances* **9**, eadg8340 (2023).

[14] Cooley, S. W. *et al.* Coldest canadian arctic communities face greatest reductions in shorefast sea ice. *Nature Climate Change* **10**, 533–538 (2020).

[15] Laidler, G. J. *et al.* Travelling and hunting in a changing arctic: Assessing inuit vulnerability to sea ice change in igloolik, nunavut. *Climatic change* **94**, 363–397 (2009).

[16] Laidre, K. L. *et al.* Glacial ice supports a distinct and undocumented polar bear subpopulation persisting in late 21st-century sea-ice conditions. *Science* **376**, 1333–1338 (2022).

[17] Itkin, P., Losch, M. & Gerdes, R. Landfast ice affects the stability of the Arctic halocline: Evidence from a numerical model. *Journal of Geophysical Research: Oceans* **120**, 2622–2635 (2015).

[18] Sterlin, J. *et al.* Influence of the representation of landfast ice on the simulation of the Arctic sea ice and Arctic Ocean halocline. *Ocean Dynamics* **74**, 407–437 (2024).

[19] Martinson, D. G. & Iannuzzi, R. A. Spatial/temporal patterns in Weddell gyre characteristics and their relationship to global climate. *Journal of Geophysical Research: Oceans* **108** (2003).

[20] Beer, E., Eisenman, I., Wagner, T. J. & Fine, E. C. A possible hysteresis in the Arctic Ocean due to release of subsurface heat during sea ice retreat. *Journal of Physical Oceanography* **53**, 1323–1335 (2023).

[21] Polyakov, I. V., Pnyushkov, A. V. & Carmack, E. C. Stability of the Arctic halocline: a new indicator of Arctic climate change. *Environmental Research Letters* **13**, 125008 (2018).

[22] Polyakov, I. V. *et al.* Greater role for Atlantic inflows on sea-ice loss in the Eurasian Basin of the Arctic Ocean. *Science* **356**, 285–291 (2017).

[23] Steele, M. & Boyd, T. Retreat of the cold halocline layer in the Arctic Ocean. *Journal of Geophysical Research: Oceans* **103**, 10419–10435 (1998).

[24] Newton, R., Schlosser, P., Martinson, D. G. & Maslowski, W. Freshwater distribution in the arctic ocean: simulation with a high-resolution model and model-data comparison. *Journal of Geophysical Research: Oceans* **113** (2008).

[25] Martinson, D. G. & Steele, M. Future of the arctic sea ice cover: Implications of an antarctic analog. *Geophysical Research Letters* **28**, 307–310 (2001).

[26] Behrendt, A., Sumata, H., Rabe, B. & Schauer, U. A comprehensive, quality-controlled and up-to-date data set of temperature and salinity data for the Arctic Mediterranean Sea (Version 1.0) (2017).

[27] Behrendt, A., Sumata, H., Rabe, B. & Schauer, U. UDASH–Unified Database for Arctic and Subarctic Hydrography. *Earth System Science Data* **10**, 1119–1138 (2018).

[28] Paffrath, R., Laukert, G., Bauch, D., Rutgers van der Loeff, M. & Pahnke, K. Separating individual contributions of major Siberian rivers in the Transpolar Drift of the Arctic Ocean. *Scientific Reports* **11**, 1–11 (2021).

[29] Olason, E. A dynamical model of Kara Sea land-fast ice. *Journal of Geophysical Research: Oceans* **121**, 3141–3158 (2016).

[30] Asbjørnsen, H., Årthun, M., Skagseth, Ø. & Eldevik, T. Mechanisms underlying recent Arctic Atlantification. *Geophysical research letters* **47**, e2020GL088036 (2020).

[31] Ingvaldsen, R. B. *et al.* Physical manifestations and ecological implications of Arctic Atlantification. *Nature Reviews Earth & Environment* **2**, 874–889 (2021).

[32] Duan, C., Dong, S., Xie, Z. & Wang, Z. Temporal variability and trends of sea ice in the Kara Sea and their relationship with atmospheric factors. *Polar Science* **20**, 136–147 (2019).

[33] Zatsepin, A. *et al.* On the mechanism of wind-induced transformation of a river runoff water lens in the Kara Sea. *Oceanology* **57**, 1–7 (2017).

[34] Zhang, J., Lindsay, R., Schweiger, A. & Steele, M. The impact of an intense summer cyclone on 2012 Arctic sea ice retreat. *Geophysical Research Letters* **40**, 720–726 (2013).

[35] Parkinson, C. L. & Comiso, J. C. On the 2012 record low Arctic sea ice cover: combined impact of preconditioning and an August storm. *Geophysical Research Letters* **40**, 1356–1361 (2013).

[36] Janout, M. A. *et al.* Kara Sea freshwater transport through Vilkitsky Strait: variability, forcing, and further pathways toward the western Arctic Ocean from a model and observations. *Journal of Geophysical Research: Oceans* **120**, 4925–4944 (2015).

[37] Wang, Q., Danilov, S., Sidorenko, D. & Wang, X. Circulation pathways and exports of Arctic river runoff influenced by atmospheric circulation regimes. *Frontiers in Marine Science* **8**, 707593 (2021).

[38] Laukert, G. *et al.* Ocean circulation and freshwater pathways in the Arctic Mediterranean based on a combined Nd isotope, REE and oxygen isotope section across Fram Strait. *Geochimica et Cosmochimica Acta* **202**, 285–309 (2017).

[39] Janout, M. A. *et al.* On the variability of stratification in the freshwater-influenced Laptev Sea region. *Frontiers in Marine Science* **7**, 543489 (2020).

[40] Peralta-Ferriz, C. & Woodgate, R. A. Seasonal and interannual variability of pan-Arctic surface mixed layer properties from 1979 to 2012 from hydrographic data, and the dominance of stratification for multiyear mixed layer depth shoaling. *Progress in Oceanography* **134**, 19–53 (2015).

[41] Marshall, J., Adcroft, A., Hill, C., Perelman, L. & Heisey, C. A finite-volume, incompressible navier stokes model for studies of the ocean on parallel computers. *Journal of Geophysical Research: Oceans* **102**, 5753–5766 (1997).

[42] MITgcm Group. MITgcm User Manual. https://mitgcm.readthedocs.io/ (2022).

[43] Semtner, A. J. A model for the thermodynamic growth of sea ice in numerical investigations of climate. *Journal of Physical Oceanography* **6**, 379–389 (1976).

[44] Hibler, W. D. A dynamic thermodynamic sea ice model. *Journal of Physical Oceanography* **9**, 815–846 (1979).

[45] Zhang, J. & Hibler, W. D. On an efficient numerical method for modeling sea ice dynamics. *Journal of Geophysical Research: Oceans* **102**, 8691–8702 (1997).

[46] Dee, D. P. *et al.* The ERA-Interim reanalysis: configuration and performance of the data assimilation system. *Quarterly Journal of the Royal Meteorological Society* **137**, 553–597 (2011).

[47] Steele, M., Ermold, W. & Zhang, J. Modeling the formation and fate of the near-surface temperature maximum in the Canadian Basin of the Arctic Ocean. *Journal of Geophysical Research: Oceans* **116**, 1–13 (2011).

[48] Losch, M., Menemenlis, D., Campin, J. M., Heimbach, P. & Hill, C. On the formulation of sea-ice models. Part 1: Effects of different solver implementations and parameterizations. *Ocean Modelling* **33**, 129–144 (2010).

[49] Ungermann, M. & Losch, M. An observationally based evaluation of subgrid scale ice thickness distributions simulated in a large-scale sea ice-ocean model of the Arctic Ocean. *Journal of Geophysical Research: Oceans* **123**, 8052–8067 (2018).